

A New Approximation for 3D Electromagnetic Scattering in the Presence of Anisotropic Conductive Media

Guo-zhong Gao

*Dept. of Petroleum and Geosystems Engr.
The University of Texas at Austin
Austin, Texas, 78712, USA
ggao@pe.utexas.edu*

Sheng Fang

*Baker Atlas
2001 Rankin Rd.
Houston, TX, 77073, USA
sheng.fang@bakeratlas.com*

Carlos Torres-Verdín

*Dept. of Petroleum and Geosystems Engr.
The University of Texas at Austin
Austin, Texas, 78712, USA
cverdin@uts.cc.utexas.edu*

SUMMARY

Accurate and efficient modeling of three-dimensional (3D) electromagnetic (EM) scattering remains an open challenge in the presence of anisotropic conductive media. Numerical algorithms used to simulate the response of dipping and anisotropic rock formations can easily exceed standard computer resources as EM fields become fully coupled in general.

In the past, several scattering approximations have been developed to efficiently simulate complex EM problems arising in the probing of subsurface rock formations. These approximations include Born, Rytov, Extended Born (ExBorn), and Quasi-Linear (QL), among others. However, so far none of these approximations has been adapted to simulate scattering in the presence of anisotropic conductive media. In this paper, we describe and benchmark a novel EM scattering approximation that remains accurate and efficient in the presence of 3D anisotropic conductive media. The approximation is based on the integral formulation of EM scattering and takes advantage of the spatial smoothness and general vectorial properties of EM fields internal to scatterers. A general vectorial formulation is used to properly account for complex EM coupling due to anisotropy.

Several numerical examples borrowed from borehole induction logging are used to describe and assess the accuracy and efficiency of the new EM scattering approximation. The approximation allows one to accurately simulate the EM response of more than 1 million cells within a few minutes of CPU time on a serial computer with standard memory and speed resources.

Key words: Integral Equation, 3D Electromagnetic Scattering, Approximation, Anisotropy

INTRODUCTION

Integral equations have been widely used to solve EM scattering problems, including those arising in geophysical

prospecting and antenna applications. Hohmann (1971) first discussed the application of integral equations to the simulation of two-dimensional (2D) subsurface geophysical problems. Since then, a number of applications and developments have been reported that include 3D EM scattering in the presence of complex geometrical structures (e.g. Hohmann, 1975, and 1983; Wannamaker, 1983; Xiong, 1992; Gao, 2002; and Fang et al., 2003; among others).

Solution of EM scattering by integral equations includes two serial steps. First, the spatial distribution of electric field within scatterers is computed through a discretization scheme. Second, the internal electric fields are "propagated" to receiver locations. It is often necessary to discretize the scatterers into a large number of cells depending on (a) frequency, (b) conductivity contrast, (c) size of the scatterers, and (d) proximity of source and/or receiver to scatterers. This discretization gives rise to a full complex matrix that needs to be inverted to obtain a solution for the spatial distribution of internal electric fields. Requirements of computer memory storage increase quadratically with an increase in the number of discretization cells. Moreover, the need to invert a large, full, and complex matrix places significant constraints to the applicability of 3D integral equation methods in the presence of complex geometrical structures.

There are several numerical strategies used to overcome the difficulties associated with integral equation formulations of EM scattering. One of these strategies, described by Fang *et al* (2003), takes advantage of the symmetry properties of Toeplitz matrices and makes use of a suitable combination of BiCGSTAB(l) (Bi-Conjugate Gradient STABlized (l)) (Gerard and Diederik, 1993) and the FFT (Fast Fourier Transform) to iteratively solve the linear system of equations. The latter method is a natural extension of the widely used CG-FFT (Conjugate Gradient-Fast Fourier Transform) (Catedra *et al.*, 1995) strategy to compute EM fields. However, numerical examples have shown that CPU execution times often remain impractical in large-scale simulation problems common to geophysical subsurface sensing. An alternative algorithmic solution is to develop an approximate solution. Several approximations to the integral equation formulation have been proposed in the past. These include Born (1933), Extended Born (Habashy *et al*, 1993; and Torres-Verdin and Habashy,

1994), and Quasi-Linear (Zhadnov and Fang, 1996). However, to date none of these approximations have been adapted to approach 3D EM scattering in the presence of anisotropic media.

The purpose of this paper is to develop and test a new 3D EM scattering approximation that remains accurate and efficient in the presence of anisotropic media and complex geometrical structures. Detection and quantitative analysis of electrical anisotropy of rock formations has attracted the attention of geophysicists for over 70 years. Some earth materials are known to exhibit inherent electrical anisotropy, while others, such as clastic sedimentary rocks, often exhibit effective electrical anisotropy due to fine internal layering. Presence of electrical anisotropy has been recognized as a potentially significant source of error in standard techniques used for the interpretation of borehole induction logging measurements. Understanding the effect of unaccounted rock anisotropy requires the ability to accurately and efficiently simulate induced EM fields in the presence of anisotropic media. The application examples considered in this paper are borrowed from the field of borehole multi-component induction logging. Structural complexity is introduced in the form of deviated wells intersecting horizontally layered rock formations.

THEORY OF INTEGRAL EQUATION MODELING

Assume an EM source exhibiting a time harmonic dependence, $e^{-i\omega t}$. The magnetic permeability of the medium equals that of free space, \mathbf{m}_0 . Thus, the integral equation for electric and magnetic fields is in general given by (Fang *et al.*, 2003)

$$\mathbf{E}(\mathbf{r}) = \mathbf{E}_b(\mathbf{r}) + \int_t \overline{\mathbf{G}}^e(\mathbf{r}, \mathbf{r}_0) \cdot \Delta \overline{\mathbf{S}} \cdot \mathbf{E}(\mathbf{r}_0) d\mathbf{r}_0, \quad (1)$$

and

$$\mathbf{H}(\mathbf{r}) = \mathbf{H}_b(\mathbf{r}) + \int_t \overline{\mathbf{G}}^h(\mathbf{r}, \mathbf{r}_0) \cdot \Delta \overline{\mathbf{S}} \cdot \mathbf{E}(\mathbf{r}_0) d\mathbf{r}_0, \quad (2)$$

where $\mathbf{E}(\mathbf{r})$ and $\mathbf{H}(\mathbf{r})$ are the electric and magnetic field vectors, respectively, at location \mathbf{r} . $\mathbf{E}_b(\mathbf{r})$ and $\mathbf{H}_b(\mathbf{r})$ are the electric and magnetic field vectors, respectively, associated with a homogeneous background medium of dielectric constant ϵ_{rb} and conductivity \mathbf{S}'_b , at location \mathbf{r} . Here the assumption is made of a homogeneous, unbounded, and isotropic background. Accordingly, the background complex conductivity is given by $\mathbf{S}_b = \mathbf{S}'_b - i\omega \mathbf{e}_{rb} \mathbf{e}_0$, and the wavenumber, k_b , of the background medium is given by $k_b^2 = i\omega \mathbf{m}_0 \mathbf{S}_b = \omega^2 \mathbf{m}_0 \mathbf{e}_0 \mathbf{e}_{rb} + i\omega \mathbf{m}_0 \mathbf{S}'_b$. At low frequencies, the expression for the background wavenumber simplifies to $k_b^2 = i\omega \mathbf{m}_0 \mathbf{S}'_b$.

The electric Green's tensor included in equations (1) and (2) can be expressed in closed form as

$$\overline{\mathbf{G}}^e(\mathbf{r}, \mathbf{r}_0) = (i\omega \mathbf{m}_0 \overline{\mathbf{I}} + \frac{1}{\mathbf{S}_b} \nabla \nabla) g(\mathbf{r}, \mathbf{r}_0), \quad (3)$$

where the scalar function $g(\mathbf{r}, \mathbf{r}_0)$ satisfies the wave equation

$$\nabla^2 g(\mathbf{r}, \mathbf{r}_0) + k_b^2 g(\mathbf{r}, \mathbf{r}_0) = -\mathbf{d}(\mathbf{r} - \mathbf{r}_0), \quad (4)$$

and whose solution can be explicitly written as

$$g(\mathbf{r}, \mathbf{r}_0) = \frac{e^{ik_b |\mathbf{r} - \mathbf{r}_0|}}{4\pi |\mathbf{r} - \mathbf{r}_0|} = \frac{e^{ik_b R}}{4\pi R}. \quad (5)$$

The magnetic Green's tensor is related to the electric Green's tensor through the expression

$$\overline{\mathbf{G}}^h(\mathbf{r}, \mathbf{r}_0) = \frac{1}{i\omega \mathbf{m}_0} \nabla \times \overline{\mathbf{G}}^e(\mathbf{r}, \mathbf{r}_0), \quad (6)$$

Finally, the tensor $\Delta \overline{\mathbf{S}} = \overline{\mathbf{S}} - \mathbf{S}_b = \Delta \overline{\mathbf{S}}' - i\omega \mathbf{m}_0 \Delta \mathbf{e}_r \mathbf{e}_0$ is the complex conductivity contrast within scatterers, with $\Delta \mathbf{e}_r = \mathbf{e}_r - \mathbf{e}_{rb}$, and $\Delta \overline{\mathbf{S}}' = \overline{\mathbf{S}}' - \mathbf{S}'_b$.

Equations (1) and (2) are Fredholm integral equations of the second kind. A solution of these equations can be obtained using the method of moments (MoM). Traditional implementations of the MoM yield a full matrix equation, which normally involves the following difficulties for large-scale numerical simulation problems: (a) matrix filling time is substantial; (b) very large memory storage; and (c) time-consuming solution of a complex linear system. For large 3D scatterers, often the solution to EM scattering cannot be approached directly using a naïve implementation of the MoM. For instance, in a case of 1 million discretization cells, 0.2 CPU seconds are needed to compute 10,000 entries (each entry is a 3 by 3 tensor) of the linear-system matrix. The table below summarizes two of the most significant computer requirements associated with this hypothetical situation. Obviously, such requirements place rather impractical constraints to most of today's computer platforms.

Matrix filling time	231.48 days
Memory storage (single complex precision)	33,527 Gigabytes

Table 1. Matrix filling time and computer storage associated with the assumption of 1 million discretization cells, and 0.2 CPU seconds needed to compute 10,000 entries (each entry is a 3 by 3 tensor) of the MoM's linear-system matrix.

A method has been used in Fang *et al.* (2003) to approach the same problem using BiCGSTAB(1) and the FFT. This method exploits the symmetry properties of Toeplitz matrices arising in the implementation of integral equation solutions with

uniform spatial grids. The properties of a Toeplitz matrix resemble those of a sparse matrix, whereupon only a relatively small portion of the matrix is required for matrix filling time and memory storage. However, in the solution of large-scale problems, such as those associated with borehole induction logging, computation times can often remain exceedingly large, of the order of hours for a single source location.

APPROXIMATIONS TO INTEGRAL EQUATIONS

The Born approximation (Born 1933) is perhaps the simplest and most widely used EM scattering approximation. It is based on the assumption that scattered electric fields inside scatterers are negligible compared to the normal/background electric fields. As a result, a linear expression is obtained to describe the relationship between the anomalous conductivity and the external EM scattered fields. The Born approximation remains accurate only for small conductivity contrasts, relatively small inhomogeneities, and low probing frequencies (Habashy *et al.*, 1993; Zhdanov and Fang, 1996; Fang and Wang, 2000; and Gao *et al.*, 2002).

An extended 3D EM Born approximation (ExBorn) was introduced by Habashy *et al.* (1993), and Torres-Verdin and Habashy (1994). This approximation has been widely used in the field of geophysical prospecting as it considerably extends the range of accuracy of a standard Born approximation. The ExBorn approximation can be viewed as the first-term approximation of the Taylor series expansion of the electric field distribution within scatterers. This is equivalent to assuming that the electric fields within scatterers are locally smooth. Numerical examples, however, have shown that when the EM source is close to the scatterers, internal electric fields can vary in an abrupt manner, thereby rendering the ExBorn approximation inaccurate (Torres-Verdin and Habashy, 2001; and Gao *et al.* 2002). Efforts have been made to improve the accuracy of the ExBorn approximation. Torres-Verdin and Habashy (2001) proposed a modified ExBorn approximation; Gao *et al.* (2002) constructed a set of natural preconditioners of the MoM's stiffness matrix and showed how different versions of such preconditioners may yield, as special cases, solutions equivalent to Born and Extended Born approximations. Recently Liu and Zhang (2001) have successfully used the ExBorn approximation as a preconditioner of the CG-FFT technique in an effort to improve the efficiency of their solvers.

The quasi-linear (QL) approximation was developed by Zhdanov and Fang (1996). It relates the background and scattering fields within a given discretization cell by a reflectivity tensor, which is assumed a smooth function of position. A least-squares minimization technique is used to solve for the reflectivity tensor. The internal scattered fields are computed using the reflectivity tensor and the background fields (Zhdanov and Fang, 1996). It has been shown that the QL approximation remains accurate and efficient for 3D modeling when the material property exhibits no anisotropy (Zhdanov and Fang, 1996). However, the scalar and diagonal

formulation of the QL approximation cannot provide accurate results for anisotropy modeling for cases in which the background/incident electric fields exhibit null components. Specifically, suppose that the background medium is homogeneous and unbounded, and that EM scattering is imposed with a z-directed magnetic dipole. Then for each cell, the z component of the background electric field (E_{bz}) will remain null regardless of the specific properties of the spatial distribution of electrical conductivity. As shown in equation (7) and (8), regardless of the nature of the reflectivity tensor (scalar or diagonal), the z-component of the total electric field (E_z) within each cell will remain null, i.e.

$$\begin{pmatrix} E_x \\ E_y \\ E_z \end{pmatrix} = \mathbf{I} \begin{pmatrix} E_{bx} \\ E_{by} \\ E_{bz} \end{pmatrix} \quad (7)$$

$$\begin{pmatrix} E_x \\ E_y \\ E_z \end{pmatrix} = \begin{bmatrix} \mathbf{I}_1 & 0 & 0 \\ 0 & \mathbf{I}_2 & 0 \\ 0 & 0 & \mathbf{I}_3 \end{bmatrix} \begin{pmatrix} E_{bx} \\ E_{by} \\ E_{bz} \end{pmatrix} \quad (8)$$

Clearly, the above formulation is not capable of providing the proper EM field coupling behaviour expected in generally anisotropic media. Now let us further explore how this zero-component affects the accuracy of the results. After the internal electric fields are computed, the scattering currents can be computed from the electric fields and the conductivity tensor, namely,

$$\mathbf{J}_s = \underline{\underline{\Delta \mathbf{s}}} \cdot \mathbf{E} \quad (9)$$

The scattered magnetic field can then be obtained at each receiver location by applying the magnetic Green's tensor on the scattering currents, i.e.

$$\mathbf{H} = \underline{\underline{\mathbf{G}}}^h \cdot \mathbf{J}_s \quad (10)$$

Expanding equation (10) yields

$$\begin{pmatrix} H_x \\ H_y \\ H_z \end{pmatrix} = \begin{bmatrix} G_{xx}^h & G_{xy}^h & G_{xz}^h \\ G_{yx}^h & G_{yy}^h & G_{yz}^h \\ G_{zx}^h & G_{zy}^h & G_{zz}^h \end{bmatrix} \begin{bmatrix} \mathbf{s}_{xx} & \mathbf{s}_{xy} & \mathbf{s}_{xz} \\ \mathbf{s}_{yx} & \mathbf{s}_{yy} & \mathbf{s}_{yz} \\ \mathbf{s}_{zx} & \mathbf{s}_{zy} & \mathbf{s}_{zz} \end{bmatrix} \begin{pmatrix} E_x \\ E_y \\ E_z \end{pmatrix} \quad (11)$$

or, in explicit form,

$$H_x = G_{xx}^h(\mathbf{s}_{xx}E_x + \mathbf{s}_{xy}E_y + \mathbf{s}_{xz}E_z) + G_{yx}^h(\mathbf{s}_{yx}E_x + \mathbf{s}_{yy}E_y + \mathbf{s}_{yz}E_z) + G_{zx}^h(\mathbf{s}_{zx}E_x + \mathbf{s}_{zy}E_y + \mathbf{s}_{zz}E_z) \quad (12)$$

$$H_y = G_{xy}^h(\mathbf{s}_{xx}E_x + \mathbf{s}_{xy}E_y + \mathbf{s}_{xz}E_z) + G_{yy}^h(\mathbf{s}_{yx}E_x + \mathbf{s}_{yy}E_y + \mathbf{s}_{yz}E_z) + G_{zy}^h(\mathbf{s}_{zx}E_x + \mathbf{s}_{zy}E_y + \mathbf{s}_{zz}E_z) \quad (13)$$

$$H_z = G_{xz}^h(\mathbf{s}_{xx}E_x + \mathbf{s}_{xy}E_y + \mathbf{s}_{xz}E_z) + G_{yz}^h(\mathbf{s}_{yx}E_x + \mathbf{s}_{yy}E_y + \mathbf{s}_{yz}E_z) + G_{zz}^h(\mathbf{s}_{zx}E_x + \mathbf{s}_{zy}E_y + \mathbf{s}_{zz}E_z) \quad (14)$$

Therefore, if $E_z=0$, then the contribution to the external magnetic field due to the presence of \mathbf{s}_{xz} , \mathbf{s}_{yz} , \mathbf{s}_{zz} will not

accounted for by the above expressions. In similar fashion, if the scatterer is isotropic, then the contributions to the external magnetic field due to the presence of G_{xz}^h , G_{yz}^h , and G_{zz}^h will remain unaccounted for by equations (12) through (14).

This paper unveils a new approximation that circumvents the construction problems associated with the QL approximation (scalar or diagonal) in the presence of electric anisotropy. Numerical examples drawn from borehole multi-component induction logging are used to evaluate the efficiency and accuracy of the new approximation.

A NEW EM SCATTERING APPROXIMATION

We express the total electric field vector within each discretization cell as the product of the magnitude of the background field and a direction vector, namely,

$$\mathbf{E} = \mathbf{d}e_b, \quad (15)$$

where

$$e_b = (\mathbf{E}_b^* \cdot \mathbf{E}_b)^{1/2}, \quad (16)$$

and

$$\mathbf{d} = \begin{pmatrix} d_x \\ d_y \\ d_z \end{pmatrix}. \quad (17)$$

The scalar factor of the product in equation (15) is used to synthesize the relative changes in magnitude of the electric field, whereas the vector factor in the same equation is used to synthesize the relative changes in the direction and phase of the electric field.

Equation (1) then becomes

$$e_b(\mathbf{r})\mathbf{d}(\mathbf{r}) = \mathbf{E}_b(\mathbf{r}) + \int_V \overline{\overline{G}}(\mathbf{r}, \mathbf{r}_0) \cdot \Delta \overline{\overline{S}} \cdot e_b(\mathbf{r}_0)\mathbf{d}(\mathbf{r}_0) d\mathbf{r}_0. \quad (18)$$

The new approximation stems directly from this last integral equation. Because e_b embodies relative changes in the magnitude of the internal electric field, it can be expected the vector \mathbf{d} to be spatially smoother than \mathbf{E} within the scatterer. Subsequently, we discretize the scatterer into a collection of blocks, each block being composed of several cells. This procedure assumes that within each block the \mathbf{d} vector is constant. Finally, a least-squares minimization approach is used to solve for the \mathbf{d} vector within a given block. A reduced linear system is then formed to solve for vector \mathbf{d} , thereby substantially decreasing memory storage and CPU time requirements. Additional savings in computer storage and CPU execution time can be obtained with the use of uniform spatial discretization schemes and a Toeplitz matrix formulation.

We now explore alternatives to further reduce repeated computations specific to the problem of borehole induction logging. It is first noted that only the conductivity distribution changes from logging point to logging point. Taking advantage of this remark, components of equation (18) independent of conductivity are first computed and stored in hard-disk memory. These components include expressions associated with background fields and Green's tensors. Subsequently, conductivity values are assigned for each cell considered by the discretization scheme. Finally, a normal linear system of equations is constructed and solved corresponding to the implementation of an over-determined least-squares optimization problem. The latter linear system is solved using BICGSTAB(l). After obtaining the direction vectors, the internal and external electric and magnetic fields are computed using the original integral equations.

The specific procedure used to implement the approximation is described in the Appendix. A final result can be expressed as a reduced linear system, namely,

$$(A - CS)d = R. \quad (19)$$

Expressions for matrices A, C, S and R in equation (19) can be found in the Appendix. By pre-multiplying matrix A^* to both side of equation (19) one obtains

$$(A^*A - A^*CS)d = A^*R. \quad (20)$$

Because A^*A , A^*C , and A^*R are all independent of conductivity, these three matrices can be stored in hard-disk memory prior to performing the computations. Specifically, when the conductivity distribution changes with a change of location of the induction-logging tool, it is only necessary to construct a new conductivity matrix. The remaining matrices included in equation (20) will not change with a change in tool location. It is also pointed out that in this paper we have adopted the use of A^* , instead of $(A-CS)^*$ in equation (20) (as required by the formal solution of a least-squares over-determined linear problem) because the entries of A^*A are much larger than those of A^*CS , whereupon the results of (20) remain accurate after such a simplifications. This additional approximation also helps one to avoid evaluating C^*C , which requires substantial computer resources.

When using uniform discretization grids, a Toeplitz matrix can be constructed for each discretization block. Subsequently, the multiplication of the Green's tensor and the background field in equation (A-6) can be performed using the FFT to compute the entries of matrix C. Details of this computation procedure can be found in Fang *et al.* (2003).

NUMERICAL EXAMPLES

Figure 1 shows the model used in this paper to test the newly developed scattering approximation. This model was adapted from an example proposed by Wang and Fang (2001) and

consists of 5 horizontal layers. The top and bottom layers of the model are isotropic and have a resistivity of 50 Ω·m. The third layer is also an isotropic layer, with a resistivity of 50 Ω·m and a thickness of 14.4 ft. The second and fourth layers are anisotropic with a horizontal resistivity of 3 Ω·m and a vertical resistivity of 15 Ω·m. Thickness of these two layers are 2.4ft and 12ft, respectively. Moreover, invasion may exist for these last two layers, with an invasion depth equal to 36 in, and with the resistivity in the invaded zone equal to 3 Ω·m. The borehole has a diameter of 9.6 in. and a resistivity of 1 Ω·m.

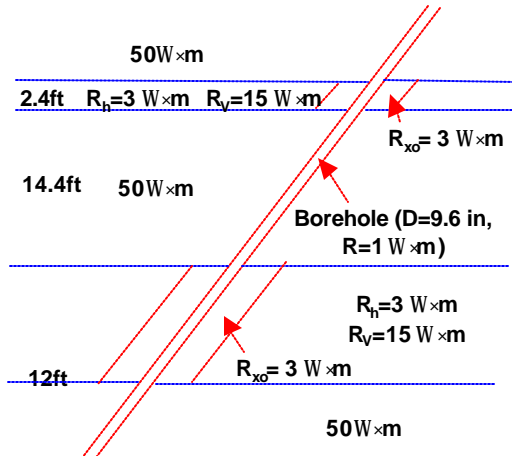


Figure 1. Diagram showing a 5-layer electrical conductivity model and associated geometrical dimensions (not to scale).

It is also assumed that the borehole may have a dip angle relative to the formation layering. Simulation results are computed for dip angles of 0 and 60 degree for two cases of rock formation model: First, the formation is assumed to exhibit no invasion and no borehole, i.e. to consist of a 1D stack of layers. A second model does assume a rock formation with borehole and invasion. Invasion and borehole parameters for this model are as described earlier. We compared simulation results with those provided by 1D code and the 3D Finite Difference Code (3D FDM in the figures) written by Wang and Fang (2001). In the descriptions and figures below, the identifier “3D IE Appr.” refers to the new approximation developed in this paper.

Figure 2 shows the borehole induction tool configuration assumed in the numerical simulations. It consists of one transmitter and two receivers moving in tandem along the borehole axis. The spacing between the transmitter and the first receiver is 1.2m (L_1), and the spacing between the transmitter and the second receiver is 1.92m (L_2). The measurement is assumed a combination of the imaginary response in the first receiver (H_1) and the second receiver (H_2), given by the formula

$$H = H_2 - \frac{L_1^2}{L_2^2} H_1 \tag{21}$$

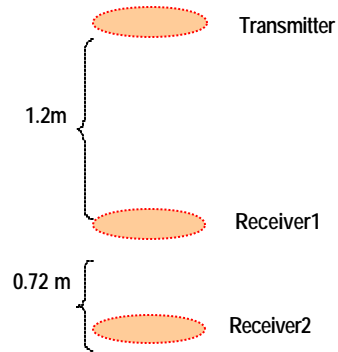


Figure 2. Assumed tool configuration for borehole induction logging (not to scale).

Figures 34 show simulation results (H_{zz} , H_{xx} , H_{yy}) obtained with the new approximation assuming a 1D rock formation with a dip angle of 0°. Simulation results for two frequencies (14KHz and 154KHz) are compared with those obtained with the 1D code. Note that H_{xx} and H_{yy} are identical when simulated along vertical wells (only one figure is shown). We comment here that H_{zz} is identical to that simulated in the corresponding isotropic formation with the horizontal conductivity values (not shown), a phenomenon customarily referred to as the “paradox of anisotropy” in induction log interpretation (Gianzero, 1999).

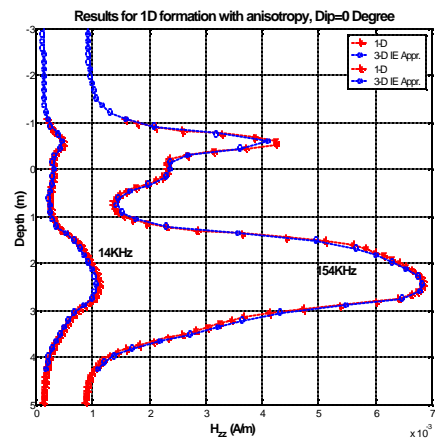


Figure 3 Comparison of the H_{zz} signal simulated with the new approximation and a 1D code assuming a 1D formation. The tool is perpendicular to the formation. Results for 14KHz and 154KHz are shown on this figure.

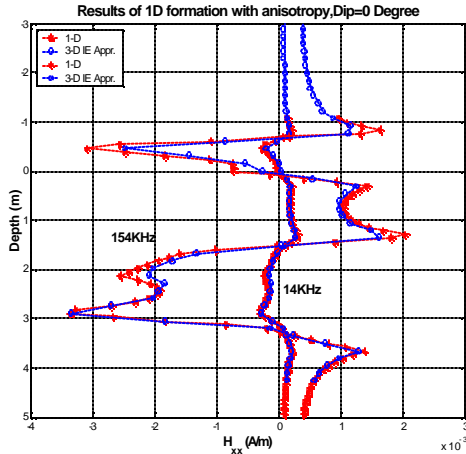


Figure 4. Comparison of the H_{xx} and H_{yy} signals simulated with the new approximation and a 1D code assuming a 1D formation. The tool is perpendicular to the formation. Results for 14KHz and 154KHz are shown on this figure. In a vertical well. H_{xx} and H_{yy} will be identical.

Figures 5-7 show simulation results (H_{zz} , H_{xx} , H_{yy}) obtained with the new approximation assuming a 1-D rock formation with a dip angle of 60° . Simulation results for two frequencies (14KHz and 154KHz) are compared with those obtained with the 1D code. Comparing Figure 3 and Figure 5 clearly show the effects of dipping on H_{zz} for both frequencies. By comparing Figure 4 and Figure 6, we can clearly see the effects (the magnitude) of the dipping on H_{xx} for both frequencies. By Comparing Figure 4 and Figure 7, we can see the even greater effects of dipping on H_{yy} for the two frequencies, both in magnitude and shape (note the effects on the thick layer).

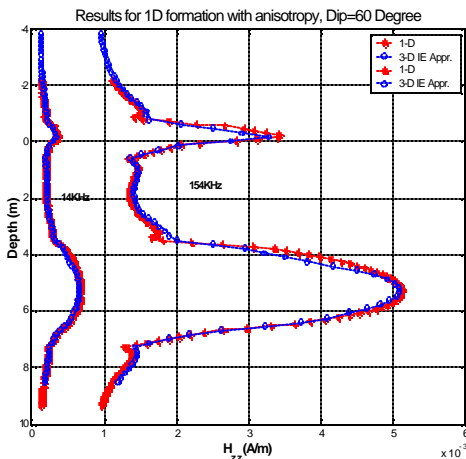


Figure 5. Comparison of the H_{zz} signal simulated with the new approximation and a 1D code assuming a 1D formation. The tool and the formation form an angle of 60° . Results for 14KHz and 154KHz are shown on this figure.

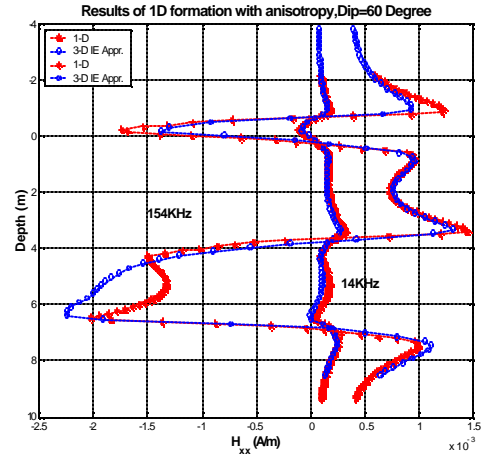


Figure 6. Comparison of the H_{xx} signal simulated with the new approximation and a 1D code assuming a 1D formation. The tool and the formation form an angle of 60° . Results for 14KHz and 154KHz are shown on this figure.

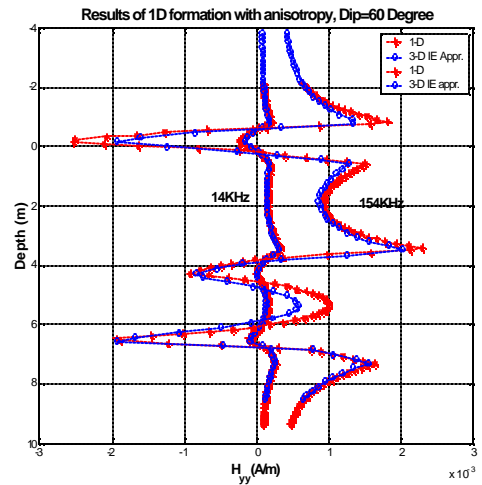


Figure 7. Comparison of the H_{yy} signal simulated with the new approximation and a 1D code assuming a 1D formation. The tool and the formation form an angle of 60° . Results for 14KHz and 154KHz are shown on this figure.

Figures 8-9 show simulation results (H_{zz} , H_{xx} , H_{yy}) obtained with the new approximation assuming a 3D rock formation (with borehole and invasion) but no dip angle. Simulation results for two frequencies (14KHz and 154KHz) are compared against those obtained with the 3D FDM code. The so-called “paradox of anisotropy” also holds in this model

example. Note the effects of borehole and invasion on H_{zz} and H_{xx} .

magnitude and shape. The effects of borehole and invasion on H_{xx} are not so manifest, however, they do have a great effects on H_{yy} (note the effects on the thick layer).

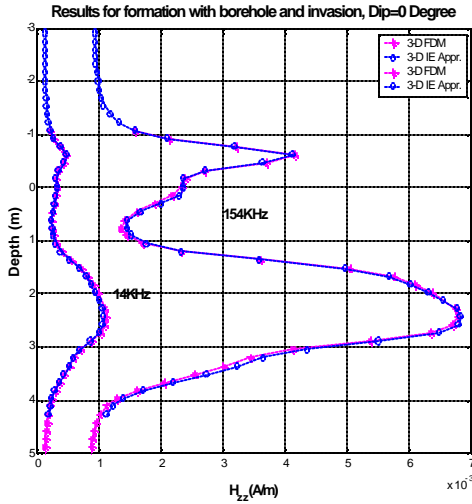


Figure 8. Comparison of the H_{zz} signal simulated with the new approximation and a 3D -FDM code assuming a 1D formation with borehole and invasion. The borehole has a dip angle of 0° . Results for 14KHz and 154KHz are shown on this figure.

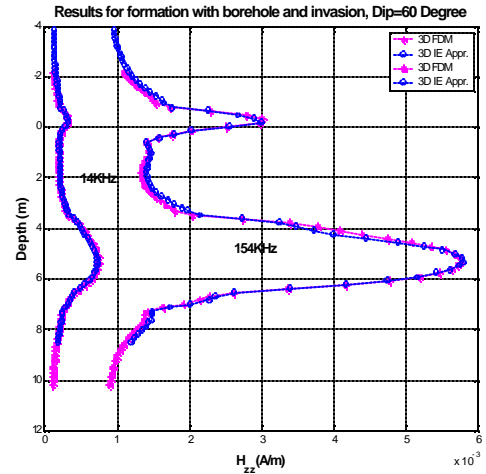


Figure 10. Comparison of the H_{zz} signal simulated with the new approximation and a 3D -FDM code assuming a 1D formation with borehole and invasion. The borehole has a dip angle of 60° . Results for 14KHz and 154KHz are shown on this figure.

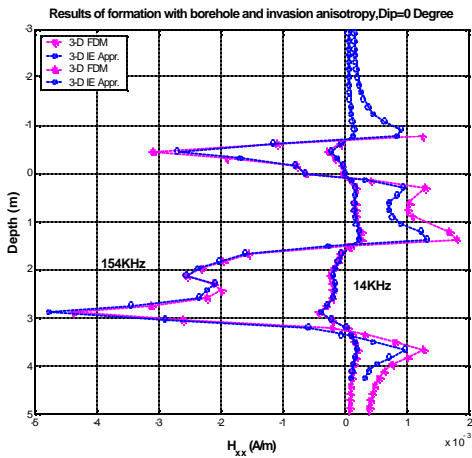


Figure 9. Comparison of the H_{xx} and H_{yy} signals simulated with the new approximation and a 3D -FDM code assuming a 1D formation with borehole and invasion. The borehole has a dip angle of 0° . Results for 14KHz and 154KHz are shown on this figure.

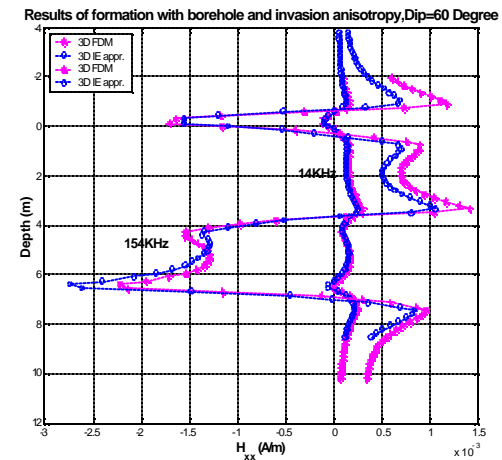


Figure 11. Comparison of the H_{xx} signal simulated with the new approximation and a 3D-FDM code assuming a 1D formation with borehole and invasion. The borehole has a dip angle of 60° . Results for 14KHz and 154KHz are shown on this figure.

Figures 10-12 show simulation results (H_{zz} , H_{xx} , H_{yy}) obtained with the new approximation assuming a 3D rock formation (borehole and invasion) and a dip angle of 60° . Simulation results for two frequencies (14KHz and 154KHz) are compared against those obtained with the 3D FDM code. Comparing Figure 5 and Figure 10, the effects of borehole and invasion can be easily seen for both frequencies, both in

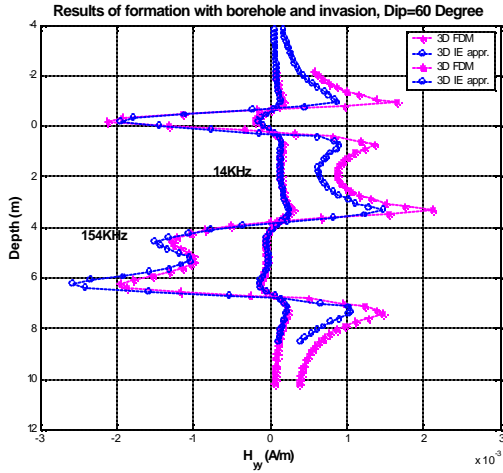


Figure 12. Comparison of the H_{yy} signal simulated with the new approximation and a 3D-FDM code assuming a 1D formation with borehole and invasion. The borehole has a dip angle of 60° . Results for 14KHz and 154KHz are shown on this figure.

The above simulation exercises consistently show that the newly developed approximation yields accurate results in the presence of reasonably complex 3D anisotropy models. Simulation results performed at low frequencies are closer to those of obtained with the 1D and 3D codes than at high frequencies. It is also noticed that at 154KHz, H_{xx} and H_{yy} exhibit large discrepancies with respect to the results provided by the 1D and 3D codes. This behavior is due to the more oscillatory nature of H_{xx} and H_{yy} at higher frequencies. All the simulations were performed with a discretization grid consisting of 100 cells in the x direction, 100 cells in the y direction, and 120 cells in the z direction. Cell size was kept uniform in the three directions and equal to 0.1 m. In total, 2400 blocks were used for the discretization of the models simulated in this paper. Simulation of electromagnetic fields for one single borehole profile location required approximately 3-4 minutes on a 900MHz Sun workstation. Wang and Fang (2001) reported 50 minutes per logging point on a power challenge R10000 processor using the 3D finite difference code.

CONCLUSIONS

This paper describes a new EM scattering approximation intended to substantially reduce computation times in the presence of complex 3D anisotropic formations. The approximation makes use of a simple vectorial product and assumes local smoothness in the vectorial properties of electric fields internal to EM scatterers. There is no need to use a Green's tensor for anisotropic media. The approximation makes use of a Green's tensor constructed under the assumption of a homogeneous isotropic background. Additional computer efficiency for the approximation is achieved assuming uniform discretization grids and by making

use of the symmetry properties of Toeplitz matrices. Numerical simulations and comparisons against 1D and 3D finite-difference codes indicate that the new approximation remains accurate within the frequency range of borehole induction tools. Moreover, the new approximation substantially improves the computer efficiency of otherwise non-approximate formulations of EM scattering. Comparisons against other integral equation approximations indicate superior accuracy and computer performance for the vectorial approximation described in this paper.

NOMENCLATURE

\mathbf{s}'	Ohmic conductivity.
\mathbf{e}_0	electrical permittivity of free space.
\mathbf{e}_r	dielectric constant.
\mathbf{m}_b	magnetic permeability of free space.
\mathbf{w}	angular frequency ($2\pi f$).
i	$=\sqrt{-1}$.
t	time.
$e^{-i\omega t}$	time convention.
$\mathbf{S} = \mathbf{s}' - i\omega \mathbf{e}_r \mathbf{e}_0$	
$\mathbf{r} = (x, y, z)$	Cartesian coordinates, equal to $x\hat{\mathbf{x}} + y\hat{\mathbf{y}} + z\hat{\mathbf{z}}$.
*	superscript, denotes conjugate transpose.
=	denotes a 3x3 tensor.
H_{xx}	= magnetic field generated in x direction by a x directed source (the second x represents the source direction).

ACKNOWLEDGMENTS

We are obliged to Dr. Tsili Wang of Baker Atlas for many useful discussions and for providing finite-difference simulation results for some of the test model examples described in this paper. A note of gratitude goes to Baker Atlas for permission to publish the results of this work. Partial support was provided by UT Austin's Research Consortium on Formation Evaluation, jointly sponsored by Baker Atlas, Halliburton, Schlumberger, and Anadarko Petroleum Corporation.

REFERENCES

- Born, M., 1933, Optics: Springer-Verlag, New York.
- Catedra, M.F., Torres, R.P., Basterrechea, J., and Gago, E., 1995, The CG-FFT method: Application of signal processing techniques to electromagnetics. Boston: Artech House.
- Fang, S., Gao, G-Z. and Torres-Verdín, C., 2003, Three-dimensional electromagnetic anisotropy modeling using integral equations, 3DEM-3 workshop, this volume.

Fang S., and Wang, T., 2000, Accurate Born simulation of induction response using an optimal background, SEG Expanded Abstract, Calgary, 1806-1809.

Gao, G-Z., 2002, 3D electromagnetic anisotropy modeling using integral equations: full and approximate solutions, applications in induction logging, Baker Atlas Reports.

Gao, G-Z. , Torres-Verdín, C., Habashy T. M. and Fang S., 2002, Numerical simulation of array induction tools with novel approximations based on an integral equation formulation, 2nd Annual Conference Report on Formation Evaluation, The University of Texas at Austin.

Gao, G-Z., Torres-Verdín, C., Habashy, T. M, and Fang, S., 2002, Approximations to electromagnetic scattering based on natural preconditioners of the method-of-moments' stiffness matrix: applications to the probing of subsurface rock formations, presented at 2002 IEEE AP-S Internat. Symp. URSI Radio Science Meeting, San Antonio, TX, June 16-21.

Gerard, L.G. Sleijpen and Diederik R. Fokkema, 1993, BiCGSTAB(l) for Linear Equations Involving Unsymmetric Matrices with Complex Spectrum, Electronic Transactions on Numerical Analysis, Vol. 1, pp.11-32.

Gianzero, S., 1999, The paradox of anisotropy revisited, The Log Analyst, Vol. 40, No. 6, P.485-491

Habashy, T.M., Groom, R.W. and Spies, B., 1993, Beyond the Born and Rytov approximations: A nonlinear approach to electromagnetic scattering, J. Geophys. Res., 98, 1759-1775.

Hohmann, G.W., 1971, Electromagnetic scattering by conductors in the earth near a line source of current: Geophysics, Vol. 36, No. 1, pp. 101-131.

Hohmann, G.W, 1975, Three-dimensional induced polarization and electromagnetic modeling: Geophysics, Vol.40, No.2, pp. 309-324.

Hohmann, G.W., 1983, Three-dimensional EM modelling, Geophys. Surv., 6, 27-53.

Klein, J.D., Martin, P.R., and Allen, D.F., 1997, the petrophysics of electrically anisotropic reservoirs: The Log Analyst, May-June.

Liu Q.H., Zhang, Z.Q., Xu, X.M., 2001, The hybrid extended Born approximation and CG-FFT method for electromagnetic induction problems, IEEE Transactions on Geoscience and Remote sensing, Vol. 39, No. 2 .

Moran, J.H. and Gianzero, S., 1979, Effects of formation anisotropy on resistivity-logging measurements: Geophysics, Vol. 44, No. 7, P.1266-1286.

Torres-Verdín, C. and Habashy, T.M., 2001, Rapid Numerical Simulation of Axisymmetric Single-well Induction Data using the Extended Born Approximation, Radio Science, Vol. 36, No. 6.

Torres-Verdín, C. and Habashy, T.M., 1994, Rapid 2.5-dimensional forward modeling and inversion via a new nonlinear scattering approximation, Radio Science, Vol. 29, No. 4, P1051-1079.

Wang T. and Fang S., 2001, 3-D electromagnetic anisotropy modeling using finite differences, Geophysics Vol. 66, No.5 P. 1386-1398.

Wannamaker, P.E., Hohmann, G.W., SanFilipo, W.A., 1983, Electromagnetic modelling of three-dimensional bodies in layered earths using integral equations, Geophysics, Vol. 49, No. 1, pp. 60-74.

Xiong, Z., 1992, Electromagnetic modeling of 3Dstructures by the method of system iteration using integral equations: Geophysics, Vol. 57, No. 12, P.1556-1561.

Zhdanov M. S. and Fang S., 1996, Quasi-linear approximation in 3-D electromagnetic modeling: Geophysics, Vol. 61, No. 3, P.646-665.

APPENDIX: ALGORITHMIC IMPLEMENTATION OF THE NEW EM SCATTERING APPROXIMATION

In order to form the reduced linear system, first divide the scattering domain into N blocks, with V_n being the volume of each block, and

$$\mathbf{d}(\mathbf{r}) = \sum_{n=1}^N \mathbf{d}_n P_n(\mathbf{r}), \quad (\text{A-1})$$

$$\text{where } P_n(\mathbf{r}) = \begin{cases} 1 & \mathbf{r} \in V_n \\ 0 & \text{elsewhere} \end{cases}.$$

Substituting equation (A-1) into equation (18) yields

$$e_b(\mathbf{r})\mathbf{d}(\mathbf{r}) - \sum_{n=1}^N \int_{V_n} \overline{\overline{G}}(\mathbf{r}, \mathbf{r}_0) \cdot e_b(\mathbf{r}_0) \Delta \overline{\overline{S}}(\mathbf{r}_0) d\mathbf{r}_0 \mathbf{d}_n = \mathbf{E}_b(\mathbf{r}). \quad (\text{A-2})$$

Because the conductivity tensor is constant within a given block one can rewrite equation (A-2) as

$$e_b(\mathbf{r})\mathbf{d}(\mathbf{r}) - \sum_{n=1}^N \int_{V_n} \overline{\overline{G}}(\mathbf{r}, \mathbf{r}_0) \cdot e_b(\mathbf{r}_0) d\mathbf{r}_0 \Delta \overline{\overline{S}}_n \mathbf{d}_n = \mathbf{E}_b(\mathbf{r}). \quad (\text{A-3})$$

Now divide block V_n into P_n cells; equation (A-3) becomes

$$e_b(\mathbf{r}_m)\mathbf{d}(\mathbf{r}_m) - \sum_{n=1}^N \left[\sum_{p=1}^{P_n} \int_{V_n^p} \overline{\overline{G}}(\mathbf{r}_m, \mathbf{r}_0) d\mathbf{r}_0 e_b^p \right] \Delta \overline{\overline{S}}_n \mathbf{d}_n = \mathbf{E}_b(\mathbf{r}_m), \quad (\text{A-4})$$

with

$$G = [G_{ij}]_{3 \times 3} = \int_{V_n^e} \overline{\mathbf{G}}^e(\mathbf{r}_m, \mathbf{r}_0) d\mathbf{r}_0 = \begin{bmatrix} G_{xx} & G_{xy} & G_{xz} \\ G_{yx} & G_{yy} & G_{yz} \\ G_{zx} & G_{zy} & G_{zz} \end{bmatrix}. \quad (\text{A-5})$$

For each cell,

$$B = [B_{ij}]_{3 \times 3} = G e_b^p = \begin{bmatrix} G_{xx} e_b^p & G_{xy} e_b^p & G_{xz} e_b^p \\ G_{yx} e_b^p & G_{yy} e_b^p & G_{yz} e_b^p \\ G_{zx} e_b^p & G_{zy} e_b^p & G_{zz} e_b^p \end{bmatrix}. \quad (\text{A-6})$$

Equation (A-4) then becomes

$$e_b(\mathbf{r}_m) \mathbf{d}(\mathbf{r}_m) - \sum_{n=1}^N \left[\sum_{p=1}^{P_n} B_n^p \right] \Delta \overline{\mathbf{S}}_n \mathbf{d}_n = \mathbf{E}_b(\mathbf{r}_m). \quad (\text{A-7})$$

Using matrix notation, equation (A-7) can be written as

$$(A_{3M \times 3N} - C_{3M \times 3N} S_{3N \times 3N}) d_{3N \times 1} = R_{3M \times 1}, \quad (\text{A-8})$$

where M, N are the number of cells and blocks, respectively, and

$$A = \begin{bmatrix} A_{11} & & & & \\ & A_{22} & & & \\ & & \dots & & \\ & & & A_{N-1, N-1} & \\ & & & & A_{NN} \end{bmatrix}. \quad (\text{A-9})$$

In the above equation, each submatrix A_i , $i=1 \dots N$ is associated with the background fields within a given block, and has dimensions $3P_n \times 3$. For example,

$$A_{11} = \begin{bmatrix} e_b^{p_1} & 0 & 0 \\ 0 & e_b^{p_1} & 0 \\ 0 & 0 & e_b^{p_1} \\ \vdots & \vdots & \vdots \\ e_b^{p_{P_1}} & 0 & 0 \\ 0 & e_b^{p_{P_1}} & 0 \\ 0 & 0 & e_b^{p_{P_1}} \end{bmatrix}, \quad (\text{A-10})$$

$$d = (d_{1x}, d_{1y}, d_{1z}, \dots, d_{Nx}, d_{Ny}, d_{Nz})^T, \quad (\text{A-11})$$

and

$$C = \begin{bmatrix} C_{11} & C_{12} & \dots & C_{1N-1} & C_{1N} \\ C_{21} & C_{22} & \dots & C_{2N-1} & C_{2N} \\ \dots & \dots & \dots & \dots & \dots \\ C_{M-11} & C_{M-12} & \dots & C_{M-1N-1} & C_{M-1N} \\ C_{M1} & C_{M2} & \dots & C_{MN-1} & C_{MN} \end{bmatrix}. \quad (\text{A-12})$$

Each submatrix $C_{ij} = [C_{ij}]_{3 \times 3} = \sum_p^{P_j} B^p$ is the contribution on cell i from block j.

Also,

$$S = \begin{bmatrix} S_{11} & & & & \\ & S_{22} & & & \\ & & \dots & & \\ & & & S_{N-1, N-1} & \\ & & & & S_{NN} \end{bmatrix}, \quad (\text{A-13})$$

where each submatrix S_i , $i=1 \dots N$ contains the average conductivity tensor for each coarse cell. The size of this submatrix is 3×3 , namely, $S_{ii} = \Delta \overline{\mathbf{S}}_i$. The conductivity averaging technique used to assemble the entries S_{ii} is the one described by Wang and Fang (2001). Finally,

$$R = (E_{b1x}, E_{b1y}, E_{b1z}, \dots, E_{bMx}, E_{bMy}, E_{bMz})^T. \quad (\text{A-14})$$